RSC Advances

PAPER

View Article Online
View Journal | View Issue

Cite this: *RSC Adv.*, 2017, **7**, 51199

Influence of interfering anions on Cu^{2+} and Zn^{2+} ions removal on chestnut outer shell-derived hydrochars in aqueous solution

Xiaoting Hong,[a]* Chengran Fang,[a] K. S. Hui,[b] K. N. Hui,[c] Haifeng Zhuang,[a] Wanpeng Liu[a] and Shengdao Shan*[a]

Received 19th September 2017
Accepted 30th October 2017

DOI: 10.1039/c7ra10384k

rsc.li/rsc-advances

Hydrothermal carbonization method was used to produce different hydrochars from chestnut outer shell at various temperatures while resolving the environmental issues of agricultural bio-waste. Hydrochars were adopted as adsorbents to remove heavy metal ions (copper and zinc ions) from aqueous solution. Hydrochar samples were characterized by Scanning Electron Microscope (SEM), Fourier Transform Infrared (FTIR), and Brunauer–Emmett–Teller (BET) nitrogen adsorption–desorption isotherm. An increase in the hydrothermal temperature from 160 °C to 220 °C results in higher BET surface area (18.81 m^2 g^{-1}) and the porosity of the samples. The resultant hydrochar at 220 °C exhibited a more excellent adsorption performance (8.13 mg g^{-1} for copper nitrate) than the other two hydrochars at low hydrothermal temperature. The current study addressed the influence of interfering anions of nitrates, sulfates and chlorides on the adsorption performance. The result shows that the hydrochar possesses larger removal efficiency for heavy metal nitrates that that of chlorides and sulfates.

1. Introduction

China is a traditional agricultural country with a considerable amount of crops. The production of agricultural wastes increases rapidly with population growth and development of agriculture. Economic crop production has become one of the fastest growing sectors of the agricultural economy, which is driven primarily by a growing demand for vegetable protein from an increasing global population. Thus, large quantities of agricultural waste are accumulated from croplands. China has the biggest chestnut production in the world, currently accounting for more than ~70% of the global production. The chestnut is a traditional fruit in China, and the outer shells have been responsible for ~2 million tons of biowaste annually in recent years. Targeted laws and regulations for the treatment and recycling of considerable amounts of chestnut outer shell wastes are insufficient in China. Direct combustion and arbitrary discarding seriously threaten the rural ecological environment and improvement in agricultural production. Agricultural biomass wastes are a huge resource because they comprise hemicellulose and lignin which have been widely used to prepare activated carbons.[1] Therefore, chestnut outer shell constitutes an interesting potential alternative to carbon adsorbent precursors, especially because of its low cost and ready availability in large quantities. The use of chestnut outer shell would contribute to the waste valorization.

Therefore, an effective transformation method for agricultural waste recycling and utilization is important in controlling serious environmental pollution and energy crisis. Traditionally, direct thermal pyrolysis was used for biochar production because of its high carbonization efficiency.[2] However, direct pyrolysis of fresh biomass is no longer favorable because of high moisture content of undried biomass. Furthermore, direct pyrolysis has low thermal-energy recovery and causes environmentally unfriendly emissions such as CO_2 and biomass fuel smoke. To overcome these complexities, finding a facile and economical route to comprehensively utilize the natural biomass is required. An alternative technology of hydrothermal carbonization (HTC) which is more energetically favorable than dry pyrolysis processes, has been increasingly employed to convert the natural biomass directly to the valuable carbon material of hydrochar.[3]

Hydrochars derived from rice straw and pig manure at 180–300 °C and biochars from the same precursors at 300–700 °C were comparatively investigated, and the results provide a promising disposal and utilization method for agricultural biowaste.[4] The effects of treatment temperature and residence time on yields and chemical properties of hydrochars were investigated during the process of hydrothermal carbonization of poultry litter. The yield and physicochemical properties of

[a]*School of Civil Engineering and Architecture, Key Laboratory of Recycling and Eco-treatment of Waste Biomass of Zhejiang Province, Zhejiang University of Science and Technology, Hangzhou 310023, China. E-mail: hanren.xiaoting@gmail.com; shanshd@vip.sina.com; Fax: +86 0571 81315186; Tel: +86 0571 85070528*

[b]*School of Mathematics, University of East Anglia, Norwich NR4 7TJ, UK*

[c]*Institute of Applied Physics and Materials Engineering, University of Macau, Avenida da Universidade, Taipa, Macau, China*

eucalyptus bark based hydrochars were optimized by controlling the process conditions, *i.e.*, carbonization temperature and residence time.[5] Wood sawdust was utilized to produce monodispersed carbonaceous microspheres by a novel hydrothermal method, combining hydrothermal carbonization and hydrothermal extraction.[6] The effect of hydrothermal conditions on the physico-chemical properties of bamboo sawdust derived hydrochars was explored based on the feasibility of using hydrochar adsorbents for adsorption of hazardous substances (Congo red and 2-naphthol) from aqueous solutions.[7]

Trace elements (copper and zinc) are essential dietary components for livestock growth. Therefore, they are inevitably used as livestock supplements in practical feeding. Any oversupplied amounts of zinc and copper doses are excreted *via* feces and urine. A wide diversity of liquid fertilizers and composts produced by the livestock manure in China are commonly applied to agricultural lands as alternative to the chemical fertilizers, which can improve the soil structure and fertility and supply valuable quantities of natural nutrients to the growing crops. Thus, the input requirement of mineral fertilizer is reduced. However, these trace elements (copper and zinc) in manure-based fertilizers can accumulate in the soil environment, which severely threatens the soil environment because of the strong toxicity of heavy metals. In recent years, biomass waste-derived hydrochars have received considerable interest as effective and environmentally friendly adsorbents for the advanced treatment of different heavy metals.[8,9]

Swine manure-derived hydrochars were applied to remove antimony(III) and cadmium(II) ions from aqueous solution. They showed high maximum adsorption capacities (19.80–27.18 mg g^{-1} for Cd(II) ions, and 2.24–3.98 mg g^{-1} for Sb(III) ions) through electrostatic adsorption and surface complexation.[10] In an aqueous environment various agricultural waste-based hydrochars exhibited an enhanced Pb(II) ion sorption capacity from 27.8 mg g^{-1} to 137 mg g^{-1} by chemical modification using KOH solution and from 0.88 mg g^{-1} to 22.82 mg g^{-1} by hydrogen peroxide modification.[11,12] Meanwhile, the heavy metal removal ability of hydrochars follows the order of $Pb^{2+} > Cu^{2+} > Cd^{2+} > Ni^{2+}$.[12] Hydrochars from biogas residues were also utilized as the support for Ni/Fe bimetallic nanoparticles and the hybrid composites acted as effective adsorbents to remove the Pb(II) ions from aqueous solutions with a removal rate of 99.5% in 1.5 h.[13]

Although surface modification was obtained and composite material facilitates the heavy metal adsorption on hydrochars, the cost is greatly increased and the application may be detrimental to the environment because of the potential variation of pH value. Many studies have been conducted to investigate the effects of various parameters such as pH, initial concentration, current density, and conductivity on the adsorption performance of hydrochars. However, little is known about the anion's effect on metal ions removal by hydrochar adsorbents.[9,14–16]

The objectives of this study include producing hydrochars with high adsorption capacities from agricultural biomass wastes and investigating the effectiveness of hydrochar as sorbents in removing Zn(II) and Cu(II) from wastewater by comparing the differences in sorption capacity between chlorate and sulfate. The adsorption performance and mechanisms responsible for heavy metal ion removal were elucidated on three different hydrochars using batch sorption isotherms. Pure hydrochar may be an effective, less costly, and environmentally sustainable adsorbent for many environmental applications, particularly with respect to metal immobilization in soil.

2. Materials and methods

2.1. Materials

Chemical reagents that were used in this study were available commercially. Zinc chloride ($ZnCl_2$, AR, purity ≥ 98.0%), zinc sulfate heptahydrate ($ZnSO_4 \cdot 7H_2O$, AR, purity ≥ 99.5%), copper chloride dehydrate ($CuCl_2$, AR, purity ≥ 98.0%), copper sulfate anhydrous ($CuSO_4$, AR, purity ≥ 99.0%), copper nitrate trihydrate ($Cu(NO_3)_2 \cdot 3H_2O$, AR, purity ≥ 99.99%), zinc nitrate hexahydrate ($Zn(NO_3)_2 \cdot 6H_2O$, AR, purity ≥ 99.99%), were purchased from Aladdin Chemical Co., Ltd., Shanghai, China. Chestnut outer shells were collected from a chestnut tree in Zhejiang University of Science and Technology.

2.2. Synthesis of hydrochars

Chestnut outer shells were pulverized by an electric disintegrator. Hydrochars were produced *via* hydrothermal reaction in a 100 mL Teflon lined autoclave reactor. Each hydrothermal reaction was carried out with a mixture of 5 g chestnut outer shell powders and 50 mL deionized water. Subsequently, autoclave was transferred into an oven and maintained at a pre-set temperature (160 °C, 190 °C, and 220 °C) under autogenous pressure for 12 h and then cooled to room temperature naturally. The resultant products were alternatively washed with deionized water and anhydrous ethanol at least thrice by extraction filtration and finally dried at 105 °C. The final chestnut outer shell-derived hydrochars were labeled as C-160, C-190, and C-220.

2.3. Characterization methods

The Brunauer–Emmett–Teller (BET) specific surface areas and average pore sizes of the resultant hydrochar samples were obtained from N_2 adsorption–desorption isotherms conducted at liquid nitrogen temperature (77 K) on the Micromeritics ASAP 2020 apparatus. The nanostructures and morphologies of the chestnut outer shell derived hydrochars were investigated by scanning electron microscope (SEM, Phenom ProX, PhenomWorld). The surface functionalities of hydrochar samples were qualitatively investigated *via* Fourier transform infrared (FTIR) spectra obtained from a Bruker Vertex 70 FTIR spectrometer in the transmittance (% *T*) mode. Hydrochar powders were mixed with potassium bromide (KBr) powder and compressed to a thin pellet for infrared examination. The analysis was carried out in the wavenumber range of 4000–400 cm^{-1}. Total elemental analyses of hydrochars were carried on Elemental Analyzer (Elementar Vario Microcube, Germany).

2.4. Adsorption experiments

The effect of contact time on the adsorption performance was carried out by adding 20 mg of each adsorbent (C-160, C-190, and C-220) into a series of 10 mL 0.12 mmol L^{-1} adsorbate aqueous solutions with Cu(II) or Zn(II) and nitrate, chloride or sulfate in flasks shaken by a shaker at a constant speed of 250 rpm. A series of flasks was taken out at different time intervals and the supernatants underwent filtration through 0.22 μm millipore filters were used to determine the concentration of the solution by atomic absorption spectroscopy (AAS, Thermo Fisher ICE 3000). Batch isotherm sorption experiments were performed by a series of adsorption using 30 mL various adsorbate aqueous solutions (0.02–0.12 mmol L^{-1}) in the presence of 60 mg of hydrochar adsorbents at a shaking speed of 250 rpm. The mixtures were then filtered after 24 h and the equilibrium concentrations of the solution C_e (mg mL^{-1}) were finally determined.

Langmuir and Freundlich adsorption models were applied to fit the adsorption isotherm curves. The Langmuir isotherm expresses monolayer adsorptions and the Freundlich is applicable to isotherm adsorption at multilayer on energetically heterogeneous surface. They can be expressed as eqn (1) and (2),[8] as follows:

$$\ln q_m = \ln k_F + \frac{1}{n} \ln C_e \quad (1)$$

$$\frac{C_e}{q_m} = \frac{C_e}{Q_e} + \frac{1}{Q_e k_L} \quad (2)$$

where C_e (mg L^{-1}) is equilibrium concentration, Q_e (mg g^{-1}) is the equilibrium adsorption capacity, and q_m (mg g^{-1}) is the maximum adsorption capacity; k_F and k_L are equilibrium adsorption constant for Langmuir and Freundlich models, respectively.

3. Results and discussion

When chestnut outer shell powder is heated to prepare hydrochar during hydrothermal reaction, the physical structure of biomass is gradually altered through reaction mechanisms in terms of hydrolysis, dehydration, decarboxylation, aromatization and re-condensation as shown in Fig. 1.[17] The surface morphologies and nanostructures of the as-prepared chestnut outer shell-derived hydrochars were firstly studied by the SEM images as shown in Fig. 2. The presence of irregular structure was observed in all samples. It can be seen from Fig. 2a shows that the original chestnut outer shell powders have dominantly fibrous structure with no evident pores on the seemingly smooth surface. By comparison, surface morphology of hydrochars was notably dependent on the heating treatment temperature. Upon hydrothermal treatment at 160 °C partial fibrous structures turned into hydrochar debris and C-160 hydrochar exhibits apparent wrinkle on the surface. With increasing the heating treatment temperature to 190 °C, original fibrous structures changed into axially-cracked structures with a large fraction of macroporous. At the highest hydrothermal temperature of 220 °C, the surfaces of C-220 hydrochars dramatically became rougher and more porous with a mesopore-dominant nanostructure. These data suggested that hydrothermal temperature played a major role in controlling the surface morphologies and nanostructures of the as-prepared chestnut outer shell-derived hydrochars.

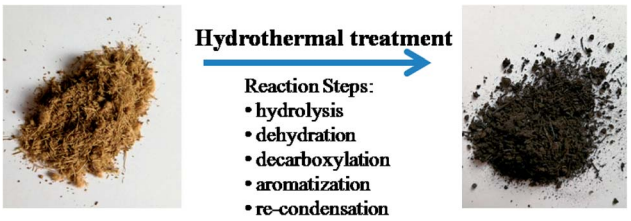

Fig. 1 Hydrochar produced from chestnut outer shell powder through hydrothermal treatment with reaction mechanisms.

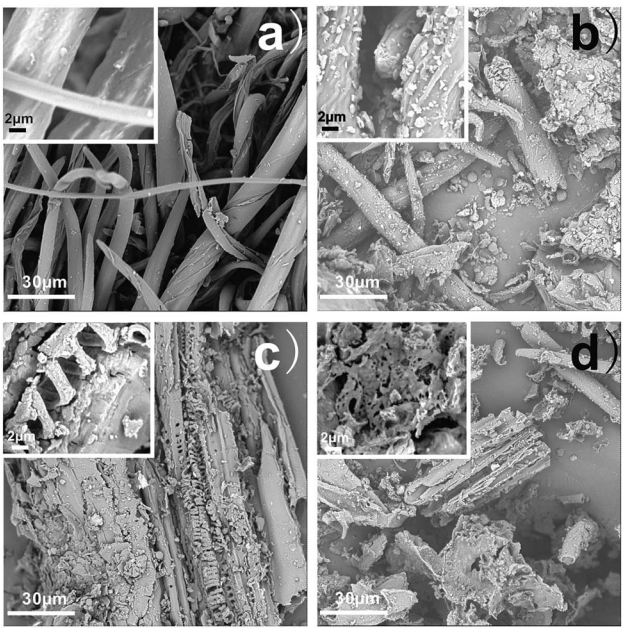

Fig. 2 SEM images of (a) chestnut outer shell powder, (b) C-160, (c) C-190, and (d) C-220 (the inset is HR-SEM image).

Table 1 lists the BET specific surface areas and average pore size of C-160, C-190, C-220, and powders of chestnut outer shell. At a low hydrothermal temperature of 160 °C, no significant difference in BET specific surface areas was found between chestnut outer shell powder (1.97 m^2 g^{-1}) and C-160 hydrochar

Table 1 BET specific surface areas and average pore size of C-160, C-190, C-220, and powders of chestnut outer shell

Samples	BET specific surface areas (m^2 g^{-1})	Average pore size (nm)
Powders of chestnut outer shell	1.97	89.5
C-160	3.12	63.5
C-190	7.91	42.7
C-220	18.81	17.1

($3.12\ m^2\ g^{-1}$). The BET surface area increased markedly to 7.91 and 18.81 $m^2\ g^{-1}$ when the hydrothermal temperature approached 190 °C and 220 °C, respectively. The average pore size of chestnut outer shell was as high as 89.5 nm. After the hydrothermal carbonization process, the average pore sizes of hydrochars decrease with the hydrothermal temperature from 63.5 nm to 17.1 nm. The results agree well with the SEM observation, where the number of pores increased on the surface of hydrochar. The hydrothermal temperature was the dominant parameter in producing the hydrochar and manipulating its surface morphology and nanostructure.[18] The increase in BET surface area and occurrence of mesopores on the hydrochar surface were either due to the decomposition of hemicellulose and cellulose of chestnut outer shell, the breaking of the hydrogen bond, or phase change within the fibrous structure in hydrothermal carbonization process.[19]

Elemental compositions, *i.e.*, C, H, O and N of C-160, C-190, C-220, and powders of chestnut outer shell are summarized in Table 2. The carbon content of hydrochar samples increased with the hydrothermal temperature, and the other elements (H, O and N) inversely decreased with the heating treatment temperature from 160 °C to 220 °C. This condition is attributed to the deoxygenating reactions (decarboxylation and dehydration reactions) during the process of hydrothermal carbonization.[20,21] A significant decrease in H/C (from 16.54 to 7.41%) and O/C (from 110.95 to 46.42%) ratios indicates a higher degree of carbonization or aromaticity due to the elimination of methyl ($-CH_3$) and ester group ($-CO_2$).[22] Conversely, high O/C ratio is the evidence of low degree of carbonization with the existence of more polar functional groups on the hydrochars.[23]

The infrared spectrum of a specific material is highly sensitive to its chemical composition based on the vibrations of atoms within the molecules. The surface functional groups of the hydrochar were investigated by the FTIR spectra. As shown in Fig. 3, all hydrochar samples exhibited similar characteristic absorption bands, thereby indicating the presence of various functional groups in the surface of biochar. A relatively strong intensity peak at a wavenumber of approximately 3428 cm^{-1} represents O–H (hydroxyl or carboxyl) stretching vibration in hydrochar surface.[24] A peak centered at 2922 cm^{-1} was attributed to the C–H stretching vibration of methyl group.[25,26] The peak at 1624 cm^{-1} was responsible for C=C and C=O stretching on the surface of hydrochar.[27,28] The signal at 1160 cm^{-1} and 1051 cm^{-1} could have arisen from C–O stretching and C–O–C symmetric stretching vibration of the hydrochars.[29,30] Among the three hydrochars, the transmittance intensities of the band of the hydrochar increased with the hydrothermal temperature such as the peaks of 3428 and 2922 cm^{-1}, due to oxygen and aromatic carbon removal in the hydrothermal carbonization process. This information also indicated the high degree of carbonization of the hydrochar sample. These results, which are derived from characteristic absorption bands, are in accordance with the previous analysis of elemental compositions.

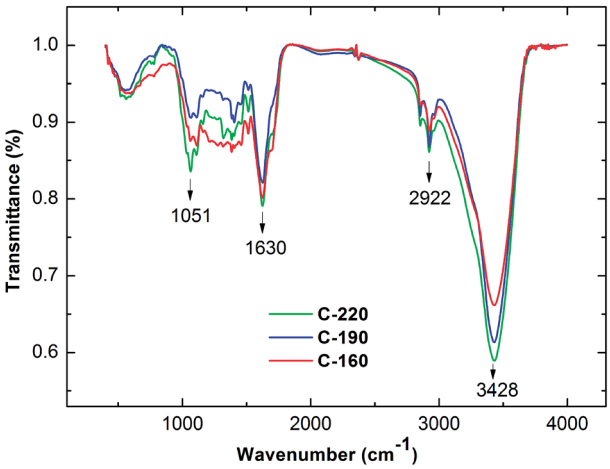

Fig. 3 FTIR spectra of C-160, C-190, and C-220 hydrochars, respectively.

The influence of anionic valence and type (NO_3^-, Cl^- and SO_4^{2-}) on the adsorption characteristics of Cu^{2+} and Zn^{2+} ions with the increase of adsorption time by C-160, C-190, and C-220 hydrochars are recorded in Fig. 4. All the experiments were carried out using 20 mg hydrochar adsorbents and the initial heavy metal concentration (Cu^{2+} and Zn^{2+}) of 0.12 mmol L^{-1} at pH of 6.5 and temperature of 25 °C. The adsorption processes underwent an analogous trend for all heavy metal ions on different hydrochars of C-160, C-190, and C-220. Evidently, the first 30 min corresponded to a rapid adsorption stage when active adsorption sites were initially dominated on the hydrochar surfaces. As the adsorption proceeded, the surface active sites were gradually occupied by heavy metal ions and became less positive. When the surface active sites are fully covered, the adsorption curves show plateaus indicating a saturated adsorption as the removal rate of heavy metal ions reaches a limit.[31] The removal rate of either Cu(II) or Zn(II) solution increases with the preparation temperature of the hydrochar, which is in accordance with previous results on the higher BET surface area and more porous structure of C-190 hydrochar. The Cu(II) removal rates with any interfering anions (nitrate, sulfate

Table 2 Elemental compositions of C-160, C-190, C-220, and powders of chestnut outer shell

Samples	C (%)	H (%)	N (%)	S (%)	O (%)
Powders of chestnut outer shell	42.21 ± 0.85	6.98 ± 0.11	2.91 ± 0.04	0.29 ± 0.01	46.83 ± 0.75
C-160	47.15 ± 0.79	5.06 ± 0.08	1.30 ± 0.03	0.19 ± 0.02	35.72 ± 0.91
C-190	52.12 ± 0.72	4.83 ± 0.06	1.09 ± 0.03	0.07 ± 0.01	31.34 ± 1.02
C-220	61.23 ± 0.82	4.54 ± 0.13	0.80 ± 0.01	0.05 ± 0.01	28.42 ± 0.83

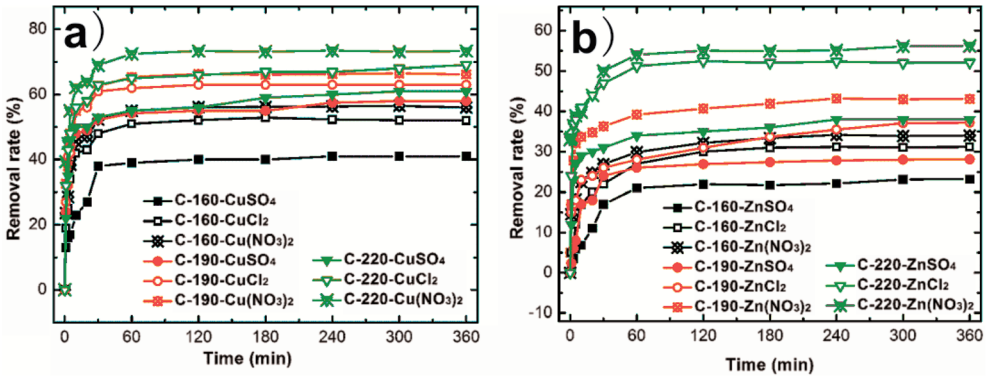

Fig. 4 Effect of contact time on Cu(II) and Zn(II) ion adsorption using C-160, C-190, and C-220, respectively.

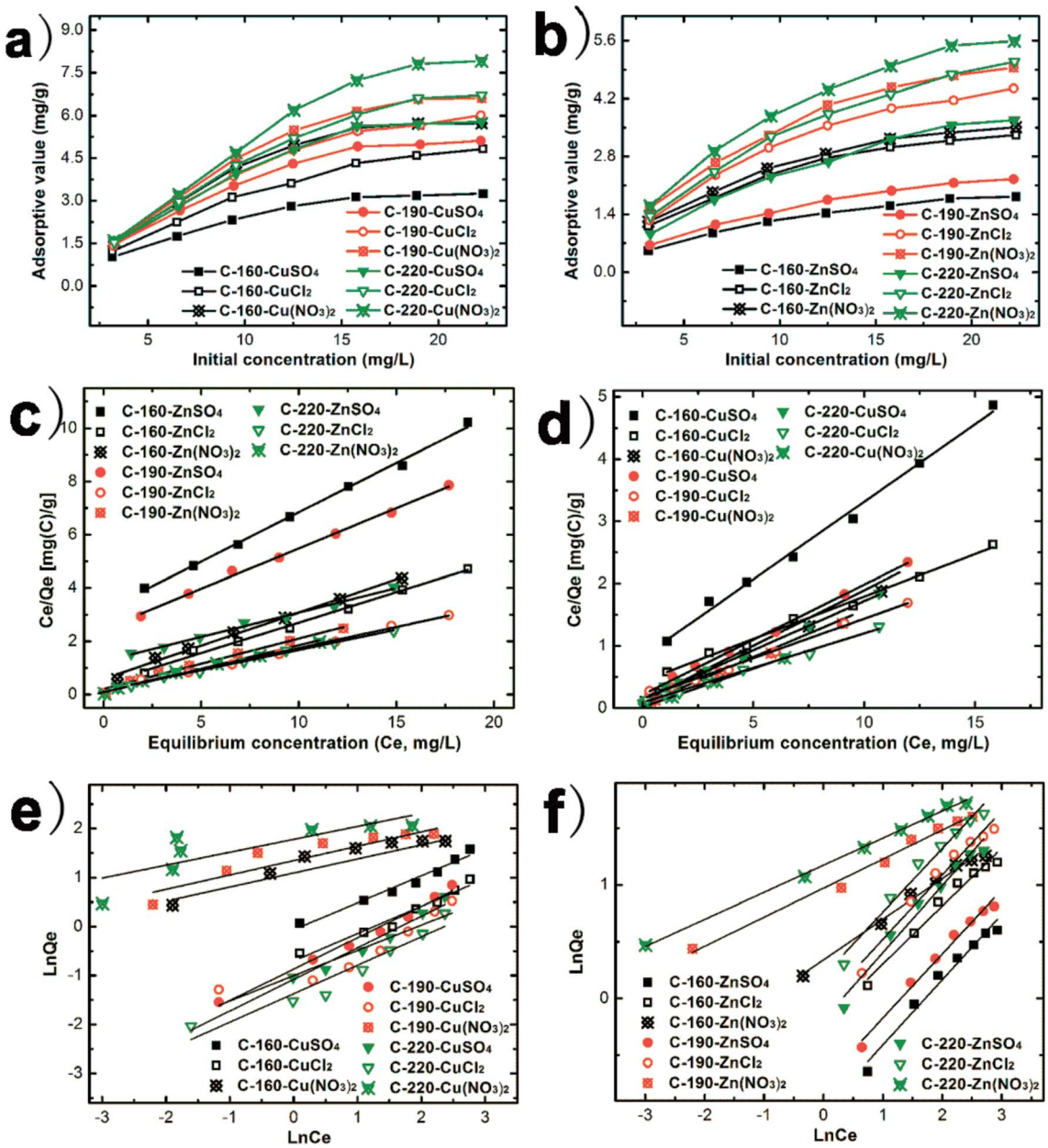

Fig. 5 (a, b) Adsorption isotherms of Cu(II) and Zn(II) ions on C-160, C-190, and C-220; (c, d) Langmuir fitted curves; (e, f) Freundlich fitted curves.

Table 3 Isotherm adsorption parameters of Cu(II) and Zn(II) ion adsorption on C-160, C-190, and C-220

		Langmuir model			Freundlich model		
Samples	Solutions	q_m (mg g^{-1})	k_L	R^2	n	k_F	R^2
C-160	$CuSO_4$ ($ZnSO_4$)	4.04(2.70)	0.30(0.12)	0.993(0.996)	1.82(1.74)	0.94(0.37)	0.965(0.972)
	$CuCl_2$ ($ZnCl_2$)	5.99(3.92)	0.33(0.34)	0.996(0.994)	1.79(1.96)	0.50(0.37)	0.956(0.971)
	$Cu(NO_3)_2$ ($Zn(NO_3)_2$)	6.07(4.03)	1.83(0.42)	0.999(0.993)	3.23(2.80)	3.26(1.41)	0.903(0.986)
C-190	$CuSO_4$ ($ZnSO_4$)	5.65(3.30)	0.82(0.12)	0.996(0.996)	1.56(1.77)	0.42(0.48)	0.985(0.984)
	$CuCl_2$ ($ZnCl_2$)	6.75(5.15)	0.76(0.43)	0.999(0.999)	1.94(1.77)	0.37(0.96)	0.848(0.964)
	$Cu(NO_3)_2$ ($Zn(NO_3)_2$)	6.92(5.29)	2.63(0.90)	0.999(0.988)	3.27(3.92)	4.06(2.64)	0.844(0.987)
C-220	$CuSO_4$ ($ZnSO_4$)	6.33(5.46)	1.13(0.15)	0.995(0.990)	1.55(1.74)	0.34(0.84)	0.980(0.971)
	$CuCl_2$ ($ZnCl_2$)	7.41(5.81)	1.18(0.48)	0.999(0.991)	1.72(1.79)	0.25(1.22)	0.913(0.973)
	$Cu(NO_3)_2$ ($Zn(NO_3)_2$)	8.13(5.88)	6.83(1.32)	0.999(0.989)	3.80(4.19)	5.94(3.23)	0.613(0.997)

and chloride) were higher than that of Zn(II) on the same hydrochar adsorbent, which is consistent with the result elsewhere.[15] The Cu(II) and Zn(II) removal efficiency varied in the range of 52–69% and 31–52%, 41–61% and 23–38%, and 56–73% and 34–56% in the presence of chloride, sulfate, and nitrate in bulk solution, respectively.

The adsorption isotherms of Cu(II) and Zn(II) ions onto C-160, C-190, and C-220 hydrochars are shown in Fig. 5, which mainly compares the adsorption of heavy metal ions as a function of different anions (nitrate, sulfate and chloride). Raw biomass of chestnut outer shell powder has the lowest adsorption capacities (not shown in Fig. 5). Fig. 5a and b show that the adsorption capacities of the three hydrochars followed the order of C-160 < C-190 < C-220 and the order of sulfate < chloride < nitrate. Notably, C-220 hydrochar exhibited the largest adsorption capacity in terms of q_m as calculated by Langmuir equation following $Cu(NO_3)_2$ (8.13 mg g^{-1}) > $CuCl_2$ (7.41 mg g^{-1}) > $CuSO_4$ (6.33 mg g^{-1}) > $Zn(NO_3)_2$ (5.88 mg g^{-1}) > $ZnCl_2$ (5.81 mg g^{-1}) > $ZnSO_4$ (5.46 mg g^{-1}). Evidently, the values of q_m were positively correlated with BET surface area and average pore size of hydrochars. The Langmuir and Freundlich models were used to fit the isotherms. The final fitting parameters from both isotherm adsorption models are summarized in Table 3. Langmuir model fitted better for the experimental equilibrium adsorption data than the Freundlich model for all curves with relative higher R^2-values as shown in Fig. 5c and d. All adsorption results indicated that the type of anions influenced significantly the removal efficiencies of Cu(II) and Zn(II) ions, where the role of nitrate ions were more considerable than that of chloride ions and sulfate ions in terms of removing metal ions.

Analogously, several authors reported that the performance of heavy metal ion removal in the chloride solution was more significant in comparison with that in sulfate solution,[32] which could be partially caused by the competitive adsorption between heavy metal ions and anions on hydrochars due to a higher molar saturation capacity of sulfate than that of chloride.[33] Moreover, comparison results between interfering ions of nitrates and chlorides shows that nitrates are more desirable anions than chlorides in the solution, because of their electronegativity impact ($-ONO_2$ > $-Cl$) on adsorption capacity.[34]

4. Conclusions

Three chestnut outer shell-derived hydrochars were prepared and characterized in terms of surface structural properties and functionaries. The hydrochar adsorbents were evaluated for the adsorption of Zn(II) and Cu(II) ions while comparing the differences in sorption capacity among nitrate, chlorate and sulfate. The Cu(II) removal rates for nitrate, sulfate and chloride were higher than that of Zn(II) on the same hydrochar. The adsorption process proceeds the quickest for the system with nitrate ions, followed by chloride ions and sulfate ions. C-220 shows the largest adsorption capacity in $CuNO_3$ solution compared to the other two hydrochars and other solutions. Langmuir model fits better for the experimental equilibrium curves than Freundlich model. The hydrochar could be an environmentally-friendly agent for water remediation or metal immobilization in soil.

Conflicts of interest

There are no conflicts to declare.

Acknowledgements

Financial support for this work was provided by the National Key R&D Program of China (13th Five Year Plan, 2017YFD061006), Natural Science Foundation of Zhejiang Province (Y18E080055), Major Science and Technology Projects of Zhejiang Province (2015C02037), and Zhejiang University of Science and Technology youth talent cultivation plan.

References

1 Z. Z. Chowdhury, S. B. Abd Hamid, M. M. Rahman and R. F. Rafique, *RSC Adv.*, 2016, **6**, 102680–102694.
2 G. Yang, Z. Wang, Q. Xian, F. Shen, C. Sun, Y. Zhang and J. Wu, *RSC Adv.*, 2015, **5**, 40117–40125.
3 C. Gai, Y. Guo, N. Peng, T. Liu and Z. Liu, *RSC Adv.*, 2016, **6**, 53713–53722.
4 Y. Liu, S. Yao, Y. Wang, H. Lu, S. K. Brar and S. Yang, *Bioresour. Technol.*, 2017, **235**, 332–337.

5 P. Gao, Y. Zhou, F. Meng, Y. Zhang, Z. Liu, W. Zhang and G. Xue, *Energy*, 2016, **97**, 238–245.
6 Q. Zheng, M. Morimoto and T. Takanohashi, *RSC Adv.*, 2017, **7**, 42123–42128.
7 Y. Li, A. Meas, S. Shan, R. Yang and X. Gai, *Bioresour. Technol.*, 2016, **207**, 379–386.
8 H. Zhang, F. Zhang and Q. Huang, *RSC Adv.*, 2017, **7**, 5790–5799.
9 Y. Lei, H. Su and R. Tian, *RSC Adv.*, 2016, **6**, 107829–107835.
10 L. Han, H. Sun, K. S. Ro, K. Sun, J. A. Libra and B. Xing, *Bioresour. Technol.*, 2017, **234**, 77–85.
11 J. T. Petrović, M. D. Stojanović, J. V. Milojković, M. S. Petrović, T. D. Šoštarić, M. D. Laušević and M. L. Mihajlović, *J. Environ. Manage.*, 2016, **182**, 292–300.
12 Y. Xue, B. Gao, Y. Yao, M. Inyang, M. Zhang, A. R. Zimmerman and K. S. Ro, *Chem. Eng. J.*, 2012, **200–202**, 673–680.
13 Z. Tang, Y. Deng, T. Luo, Y.-s. Xu and N.-m. Zhu, *Chem. Eng. J.*, 2016, **292**, 224–232.
14 A. Bogusz, P. Oleszczuk and R. Dobrowolski, *Bioresour. Technol.*, 2015, **196**, 540–549.
15 J.-H. Park, Y. S. Ok, S.-H. Kim, J.-S. Cho, J.-S. Heo, R. D. Delaune and D.-C. Seo, *Chemosphere*, 2016, **142**, 77–83.
16 J. Fang, B. Gao, J. Chen and A. R. Zimmerman, *Chem. Eng. J.*, 2015, **267**, 253–259.
17 J. Fang, L. Zhan, Y. S. Ok and B. Gao, *J. Ind. Eng. Chem.*, 2017, DOI: 10.1016/j.jiec.2017.08.026.
18 B. M. Ghanim, D. S. Pandey, W. Kwapinski and J. J. Leahy, *Bioresour. Technol.*, 2016, **216**, 373–380.
19 Y. Gao, X. Wang, J. Wang, X. Li, J. Cheng, H. Yang and H. Chen, *Energy*, 2013, **58**, 376–383.
20 S. E. Elaigwu and G. M. Greenway, *Fuel Process. Technol.*, 2016, **149**, 305–312.
21 X. Li, M.-F. Li, J. Bian, B. Wang, J.-K. Xu and R.-C. Sun, *RSC Adv.*, 2015, **5**, 77147–77153.
22 D. Xu, Y. Zhao, K. Sun, B. Gao, Z. Wang, J. Jin, Z. Zhang, S. Wang, Y. Yan, X. Liu and F. Wu, *Chemosphere*, 2014, **111**, 320–326.
23 K. Wiedner, C. Naisse, C. Rumpel, A. Pozzi, P. Wieczorek and B. Glaser, *Org. Geochem.*, 2013, **54**, 91–100.
24 L. M. Wu, D. S. Tong, C. S. Li, S. F. Ji, C. X. Lin, H. M. Yang, Z. K. Zhong, C. Y. Xu, W. H. Yu and C. H. Zhou, *Appl. Clay Sci.*, 2016, **119**, 116–125.
25 S. Ismadji, D. S. Tong, F. E. Soetaredjo, A. Ayucitra, W. H. Yu and C. H. Zhou, *Appl. Clay Sci.*, 2016, **119**, 146–154.
26 H. Huang, J. Tang, K. Gao, R. He, H. Zhao and D. Werner, *RSC Adv.*, 2017, **7**, 14640–14648.
27 Z. Chen, B. Chen and C. T. Chiou, *Environ. Sci. Technol.*, 2012, **46**, 11104–11111.
28 D. C. Li, J. W. Ding, T. T. Qian, S. Zhang and H. Jiang, *RSC Adv.*, 2016, **6**, 12226–12234.
29 J. Lee, X. Yang, S.-H. Cho, J.-K. Kim, S. S. Lee, D. C. W. Tsang, Y. S. Ok and E. E. Kwon, *Appl. Energy*, 2017, **185**, 214–222.
30 M. W. Yap, N. M. Mubarak, J. N. Sahu and E. C. Abdullah, *J. Ind. Eng. Chem.*, 2017, **45**, 287–295.
31 M. Mahramanlioglu, I. Kizilcikli and I. O. Bicer, *J. Fluorine Chem.*, 2002, **115**, 41–47.
32 J. L. Trompette and H. Vergnes, *J. Hazard. Mater.*, 2009, **163**, 1282–1288.
33 Z. Chen, H. Zhang, C. Wu, Y. Wang and W. Li, *Desalination*, 2015, **369**, 46–50.
34 A. Bogusz, P. Oleszczuk and R. Dobrowolski, *Bioresour. Technol.*, 2015, **196**, 540–549.